geologica acta

Citation: Călugăru, M.E., Munteanu, M., Wälle, M., Isac, A., 2025. Trace element contents in bornite, chalcopyrite and pyrite (LA-ICP-MS) from Miocene porphyry copper-gold deposits from Metaliferi Mountains, Romania. Geologica Acta, 23.28, 1-pgs. DOI: 10.1344/GeologicaActa2025.23.28

Online ISSN: 1696-5728

Trace element contents in bornite, chalcopyrite and pyrite (LA-ICP-MS) from Miocene porphyry copper-gold deposits from Metaliferi Mountains, Romania

Mihaela-Elena Călugăru[1] **Marian Munteanu**[1,3] **Markus Wälle**[4] **Anca Isac**[1]

[1]**Geological Institute of Romania**
Caransebeș 1 Bucharest, Romania, Călugăru E-mail: mihaela.elena.cioaca@gmail.com
Munteanu E-mail: marianmunteanu2000@gmail.co, Isac E-mail: anca.isac@igr.ro.

[2]**Institute of Geodynamics of the Romanian Academy**
Bucharest 020032, Romania

[3]**Swiss Gemmological Institute SSEF**
Basel, Switzerland. Wälle E-mail: waellemarkus@gmx.ch

ABSTRACT

In porphyry systems, valuable elements such as Au, Ag, Te, Se and Bi are found in trace contents associated with Cu and Fe sulfides. The relations between sulfide and the trace element contents, as well as the role of physicochemical factors in the uptake of different trace elements are still being assessed. This study focused on understanding how these elements are concentrated in selected sulfides (pyrite, chalcopyrite and bornite) and on the relation between the measured trace element composition of these sulfides and the hydrothermal alteration types in six porphyry deposits from Romania: Roșia Poieni, Bucium-Tarnița, Colnic, Rovina, Valea Morii and Bolcana. Based on LA-ICP-MS micro-analytical data, bornite is revealed as the main host for Bi (1077ppm), Se (810ppm), Ag (312ppm) and Te (43.73ppm). Chalcopyrite is also relatively rich in Se (199-403ppm), Ag (1.88-49.97ppm) and Te (1.95-36.06ppm). Pyrite is enriched in Co (98.81-704ppm), Ni (3.81-20.68ppm), As (2.13-166ppm), Se (24.65-729ppm) and Te (0.99-11.75ppm). These elements occur in the host sulfides as solid solution and as mineral microinclusions. Gold content is <0.2ppm in both Cu-Fe sulfides and pyrite. There is no significant variation in trace element ratio in chalcopyrite (Se/In) and in pyrite (Co/Ni, Co/Cu, Ag/Co) when comparing results from potassic-altered with chloritic-sericitic altered samples. Based on trace element results and micro-textural features of studied minerals, we suggest that these elements were initially incorporated in the crystal lattice during the potassic alteration and the overprinting of chloritic-sericitic alteration caused the exsolution and redistribution of trace elements within their host minerals.

KEYWORDS **Trace Elements. Porphyry Cu-Au. Chalcopyrite. Bornite. Pyrite.**

INTRODUCTION

Porphyry-type ore deposits are known as a major source of Cu, Au and Mo, however, other elements such as Ag, Re, Pd, Te, Se, Pb, Zn, Bi, Sb and In could reach high contents and be recovered as by-products from these deposits (Sillitoe, 2010; Sinclair, 2007). The industrial demand for many of these elements (*e.g.* Re, Ge, In, Te and PGEs) increased especially because of their use in electronics, high-temperature super alloys, green energy

devices etc. Moreover, Cu and several of the mentioned elements are classified as critical raw materials. Therefore, the interest in finding new resources of such commodities is a top priority. In porphyry-type deposits, these elements could be incorporated in the crystal lattice of several base metal ore phases and/or could be present as micro-/nano sized mineral inclusions in the common sulfides (Aird *et al.*, 2021; Cook *et al.*, 2011; Gregory *et al.*, 2013; Reich *et al.*, 2013).

The trace element signatures of sulfides could be used as tools in exploration, in the selection of the best metal recovery methods and also in understanding the ore forming processes (Brodbeck *et al.*, 2022; Cook *et al.*, 2011; Keith *et al.*, 2018, 2022; Kesler *et al.*, 2002; Reich *et al.*, 2013; Rivas-Romero *et al.*, 2021). Gold is the most important by-product of porphyry-Cu ore deposits and numerous studies have focused on the understanding of the factors and mechanisms that control gold concentration in chalcopyrite and bornite (Aird *et al.*, 2021; Gregory *et al.*, 2013; Kesler *et al.*, 2002; Simon *et al.*, 2000). Pyrite has been identified to incorporate high amounts of Au during the evolution of magmatic-hydrothermal systems, promoted by the presence of other elements, such as As, Cu, Co, Te and Se (Deditius *et al.*, 2014; Keith *et al.*, 2018; Reich *et al.*, 2013). The contents of Co, Ni, Cu, As and Ag in pyrite vary with temperature, salinity, and pH (Deditius *et al.*, 2014; Keith *et al.*, 2018; Reich *et al.*, 2013). Several trace element ratios (*e.g.* Co/Ni, Co/As, Co/Ag, Se/Ge and Se/Te) could be used to indicate physico-chemical fluid parameters and ore forming processes (Keith *et al.*, 2022; Rivas-Romero *et al.*, 2021).

Only few papers are focused on reporting the trace element geochemistry of the Neogene porphyry copper deposits from the metallogenic area of Metaliferi Mountains, Romania, mostly using bulk rock composition in sulfide rich samples (Cheşu, 1983; Cioacă *et al.*, 2014). Cheşu (1983) presents a synthesis on trace element content of several ore deposits from Romania, including the main ore deposits from Metaliferi Mountains. Cioacă *et al.* (2014) reported trace element analyses with whole rock and in situ analyses of sulfides from six deposits (Roșia Poieni, Bucium-Tarnița, Rovina, Colnic, Valea Morii and Bolcana). Textural observations and electron microprobe analyses from their study suggested that part of the Au, Ag, As, Te and Se may occur as fine-particle inclusions hosted within pyrite, chalcopyrite and bornite. Here, we present a new dataset with trace element content of Cu-Fe sulfides and pyrite from selected Romanian porphyry deposits, based on LA-ICP-MS analytic method. Based on these results, the geochemical signature of sulfides in correlation with ore assemblages and hydrothermal alteration type provided us with valuable information about the distribution of trace elements at the deposit scale. These trace elements are of high importance on the economic assessment of porphyry deposits.

GEOLOGICAL SETTING

The Metaliferi Mountains is a part of the South Apuseni Mountains, western segment of Romanian Carpathian Mountains (Fig. 1). The geology of the South Apuseni Mountains consists of a Precambrian-Palaeozoic metamorphic basement overlain by Late Jurassic to Quaternary sedimentary deposits cut by Jurassic to Pleistocene magmatic formations. The Alpine magmatism from South Apuseni Mountains is characterized by the spatial superposition of different magmatic events from Mesozoic to Cenozoic (Fig. 1): Jurassic magmatism related to the Tethyan ophiolitic suture, Late Cretaceous-Paleocene Laramian calc-alkaline magmatism developed during final stage of Tethys closure, followed by the Miocene magmatism (14.6 and ~7Ma). The last magmatism is related to the extensional activity associated to eastward translation and clockwise rotation of the Tisza-Dacia Mega Unit during collision with East European Platform (Seghedi *et al.*, 2022 and referenced therein). This magmatism is characterized by the several volcanic structures which occur along four NW-SE trending lineaments (Fig. 1). Miocene magmatic rocks display typical calc-alkaline signature, with minor occurrence of younger rocks (<12Ma) having high-K calc-alkaline affinity. From a petrographic point of view, the magmatic rocks are amphibole- and pyroxene-bearing andesites, with small volumes of basaltic andesites and dacites (Seghedi *et al.*, 2022). Many magmatic-hydrothermal ore deposits are related to volcanic structures formed during the Miocene and occur as epithermal veins, breccia pipes, and porphyry copper deposits. Most volcanic structures associated with these deposits show a specific distribution of mineralization-styles: porphyry copper-type occur at the center of the host subvolcanic intrusions, while base metal (Pb-Zn-Cu±Au, Ag) and Au-Ag±Te epithermal veins are peripheral to these (Borcoș *et al.*, 1998). Bulk rock geochemical and isotopic data suggest a mantle origin, for this source, later to be metasomatized and refertilized during subduction of neo-Tethys oceanic rocks in Mesozoic prior to extensional magma generation in the Miocene (Harris *et al.*, 2013). Seghedi *et al.* (2022) proposed that the tectonic setting during the Miocene provided the conditions for the formation of a large underplated magma chamber at the crust – mantle boundary, in response to hot upwelling convective asthenosphere. Mixing of lower crust melts and mantle melts and further crustal assimilation and minor fractional crystallization in crustal magma chambers may explain the variation in the geochemical characteristics of magmas during evolution of Miocene magmatic activity in different areas from Metaliferi Mountains.

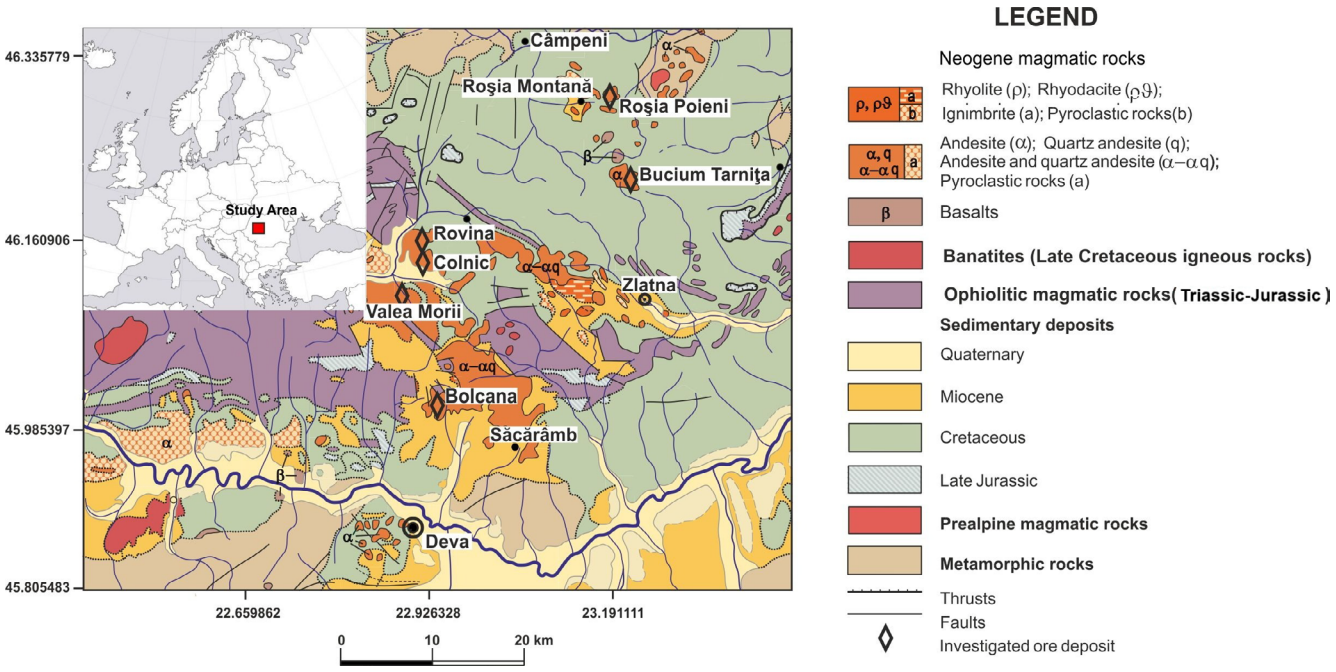

FIGURE 1. Geological map of Metaliferi Mountains with location of the investigated deposits. Modified from Geological map of the Romania 1:1000000 (Săndulescu *et al.*, 1978).

ORE DEPOSITS GEOLOGY

Porphyry deposits in the Metaliferi Mountains district (Fig. 1) are classified as Cu-Mo (Au) type (Roşia Poieni, Rovina), Cu-Au type (Valea Morii, Bolcana, and Bucium-Tarniţa) and Au-Cu type (Colnic), in according to Borcoș *et al.* (1998) and Halga *et al.* (2010).

Roşia Poieni is the largest copper ore deposit in Romania, having calculated resources of 350Mt of ore with an average grade of 0.36% Cu and 0.29g/t Au (Borcoș *et al.*, 1998). Mineralization is associated with a Miocene microdiorite subvolcanic body, which intruded Miocene andesites. The alteration zones were thoroughly presented by Milu *et al.* (2004). Potassic alteration mineral assemblage contains Mg-biotite, K-feldspar and quartz as main phases, but also chlorite, anhydrite, pyrite, chalcopyrite, magnetite, hematite, molybdenite and bornite affects the entire microdiorite body, with minor extent in the host andesite. The propylitic alteration developed in the host andesite around the microdiorite body, extending much more than the mineralized body. It generated the chloritization of the amphibole phenocrysts and groundmass, but commonly had much smaller influence on the feldspars, which can show some replacement by albite, carbonate, epidote, and sericite. Phyllic alteration overprinted the outer parts of potassic alteration zone and the inner parts of the propylitic alteration. It contains newly formed quartz, illite, phengite, illite-smectite mixed-layer minerals, smectite and kaolinite, which extensively replaced the previously formed minerals. The mineralization of phyllic alteration zone is roughly similar with that of potassic zone, with some minerals such as tetrahedrite-tennantite, sphalerite, galena and digenite also reported (Milu *et al.*, 2004). The argillic alteration overprinted the potassic, phyllic and propylitic alteration and was facilitated by the fractures from the roof of the microdiorite intrusion. Its mineral assemblage is dominated by alunite, kaolinite, dickite, pyrophyllite, diaspore, zunyite and minamiite, the associated mineralization consisting mainly of pyrite, with subordinate enargite, luzonite, marcasite, and chalcocite. High-sulfidation epithermal-style veins (enargite, luzonite, pyrite, covellite) overprint the porphyry-style mineralization (Milu *et al.*, 2004).

The Bucium-Tarniţa ore deposit (14.87-14.60Ma, Roşu *et al.*, 2004) is related to a microdiorite subvolcanic intrusion, which was emplaced at the contact between the Miocene andesites and the Cretaceous sedimentary deposits. The mineralization consists of stockworks and disseminations of magnetite, chalcopyrite, pyrite, pyrrhotite, molybdenite and native gold. These are concentrated in the core of the deposit and occur within the potassic alteration zone. Epithermal base metal veins with pyrite, sphalerite, galena, chalcopyrite, tetrahedrite-tennantite, and native gold overprint the porphyry-style mineralization (Kouzmanov *et al.*, 2005).

The Rovina Cu-Au deposit (known also as Rovina-Remetea) is associated with potassic alteration overprinted by magnetite, chlorite, epidote, K-feldspar, quartz,

anhydrite, and carbonates on an amphibole-bearing diorite porphyry. Mineralization is related to multistage intrusions, referred to as Porphyry B and Porphyry C and contains pyrite, chalcopyrite and magnetite. Typical grades range from 0.1 to 1.0g/t Au and from 0.05 to 0.70% Cu (Halga *et al.*, 2010).

The Colnic Au-Cu deposit is located at approximately 2.5km south of the Rovina deposit and consists of quartz-pyrite-chalcopyrite stockworks, developed in a small amphibole-bearing diorite porphyry. Halga *et al.* (2010) described the zonation patterns of mineralization, hydrothermal alteration, and multistage evolution of the whole system. Three types of alteration-mineralization zones are present: i) potassic alteration zone, in the central zone, which contains pyrite, chalcopyrite, pyrrhotite, magnetite and molybdenite, ii) quartz, magnetite, chlorite, epidote, carbonates, with pyrite and chalcopyrite, both being overprinted by iii) quartz-sericite alteration (*i.e.* fine-grained white mica, quartz, clay minerals) and pyrite dissemination. Mineralization grades between 0.3 and 1.3g/t Au, and 0.05 to 0.18% Cu (Halga *et al.*, 2010).

The Valea Morii porphyry Cu-Au deposit (12.8Ma, Kouzmanov *et al.*, 2003) is hosted in a quartz diorite body, which was intruded by a quartz microdioritic porphyry. The main mineralization consists of veins and disseminations of chalcopyrite and pyrite, subordinate magnetite, and bornite, all of these in association with the potassic alteration zone (potassic feldspar, chlorite, biotite, actinolite, epidote). Ore grade of the deposit is 0.26% Cu and 0.49ppm Au (André-Mayer *et al.*, 2001). Epithermal NW-trending Au-Ag vein systems telescoped the upper part of the deposit. The veins consist of sphalerite, galena, tetrahedrite, chalcopyrite, pyrite and native gold with quartz, adularia, carbonates, sericite, illite and chlorite as gangue minerals in phyllic and argillic alteration halos (André-Mayer *et al.*, 2001).

The Bolcana porphyry Cu-Au deposit is spatially and genetically related to Bolcana amphibole porphyry microdiorite intrusive complex. Several intrusive phases are described by Dénes *et al.* (2014) involving two early porphyry stocks with potassic alteration overprinted by sericite-chlorite alteration, an intermineral porphyry with moderate chlorite-sericite alteration and a late porphyry with potassic alteration overprinted by chlorite-sericite alteration. Potassic alteration is dominated by secondary biotite and potassic feldspar. Chlorite, albite, anhydrite, actinolite, and sericite are also present (Milu *et al.*, 2003). The phyllic assemblage consists of sericite, quartz and pyrite, with subordinate chlorite, anhydrite and relicts of biotite and K-feldspar (Milu *et al.*, 2003). Argillic alteration (kaolinite, smectite, mixed-layer minerals and carbonates) overprints the other alteration types (Milu *et al.*, 2003). Three mineral parageneses are described (Dénes *et al.*, 2014): i) quartz-magnetite and quartz-magnetite-pyrite-chalcopyrite-bornite as A type veins in the potassic zone of an earlier porphyry stock; ii) quartz-pyrite-chalcopyrite as A type veins with sericite-chlorite related to the intermineral porphyry stock; and iii) pyrite-chalcopyrite as D type veins which cut the late porphyry stock.

The Roșia Poieni is the only active copper mine in the area. The Bolcana deposit with inferred resources of 381 Mt at 0.53g/t Au and 0.18% Cu (Blannin *et al.*, 2021 and references therein). Both Bolcana and Valea Morii deposits are also mined in the past are now are closed. Bucium-Tarniţa deposit are explored in the past and the resource is estimated at 335Mt, with 0.50% Cu and 0.36g/t Au (Kouzmanov *et al.*, 2005). Rovina and Colnic intrusions were explored as part of the "Rovina Project", from 2004 to 2012, and currently are under the Rovina exploitation mining license (2015-2035). At Colnic, the measured and indicated resources are 133Mt, at 0.1-0.12% Cu and 0.48-0.65g/t Au, while the measured and indicated resources at Rovina are 112Mt at 0.22-0.29% Cu and 0.26-0.36g/t Au (Desautels *et al.*, 2022).

MATERIALS AND METHODS

Twelve samples from six porphyry Cu deposits were analyzed in this study (Table 1). The samples were collected from an outcrop at Colnic (COL01, COL06), from the open pit at Valea Morii (ARS03, ARS06) and at Roșia Poieni (RP01, RP05). At Rovina (ROV02, ROV04, ROV16), Bucium-Tarnița (BI07) and Bolcana (BO5002, BO1/121) samples were collected from the waste dumps of historical mining. The studied samples present characteristic porphyry-style mineralization with fine-grained disseminations and discontinuous millimetric-submillimetric sinuous veinlets of A type veins, without alteration hallo (Table 1, Fig. 2A-H). The mineralogy and petrography of the samples were determined by optical microscopy at the Geological Institute of Romania, using an Axio Imager.A2m petrographic microscope equipped with an AxioCam ICc5 digital camera. Trace element content of chalcopyrite (n= 55), pyrite (n= 29) and bornite (n= 6) were determined using a LA-ICP-MS at the Institute of Geochemistry and Petrology of ETH Zurich, using an Excimer ArF laser (193nm) for ablation of sample material, coupled with an Elan6100 DRC quadrupole ICP mass spectrometer for multi-element analysis. Isotopes of several elements (^{57}Fe, ^{56}Co, ^{60}Ni, ^{65}Cu, ^{66}Zn, ^{75}As, ^{77}Se, ^{107}Ag, ^{111}Cd, ^{115}In, ^{118}Sn, ^{121}Sb, ^{125}Te, ^{197}Au, ^{205}Tl, ^{208}Pb and ^{209}Bi) were measured in more than 130 mineral grains.

The operating conditions consisted of 100 seconds total analysis time (40s pre-ablation and 60s ablation, approximatively), 20-40μm laser spot diameter, varying

TABLE 1. Description of the samples

Deposit	Sample no.	Rock and alteration type	Mineralization	GPS coordinates
Roșia Poieni	RP01	μδ, K	Mag, Ccp, Bn (cv)	46.2322, 23.1839
	RP05	μδ, K	Mag, Ccp, Bn (cv)	
Bucium- Tarnița	BI17	μδ, K, chl.-ser. overprint	Ccp, Mag, Py	46.1585, 22.9181
Rovina	ROV02	δ, K	Py, Mag, Ccp	
	ROV04	δ, K	Py, Ccp	
	ROV16	δ, K	Py, Mag, Ccp	
Colnic	COL01	δ, K	Ccp, Py, Mag, Au	46.1183, 22.8920
	COL06	δ, K, incipient ser. overprint	Ccp (cv), Py, Mag	
Valea Morii	ARS03	μδ, K, chl.-ser. overprint	Ccp, Mag, Py	46.0837, 22.8635
	ARS06	μδ, K, chl.-ser. overprint	Ccp, Mag, Py	
Bolcana	BO-5002	μδ, K	Mag, Ccp (Bn), Bn	46.0026, 22.9329
	BO-1/121	μδ, K	Mag, Ccp (Bn), Bn	

Abbreviations: Au= Gold, Bn= Bornite, chl-ser= chloritic-sericitic alteration, Cpy= Chalcopyrite, Cv= Covellite, K= potassic alteration, Mt= Magnetite, Py= Pyrite, μδ= Microdiorite, δ= Diorite

with the size of the analyzed grains. The SILLS software (Guillong *et al.*, 2008) was used for data reduction and concentration calculation of transient LA-ICP– MS signals. Quantitative results were calibrated using MASS-1 and NIST 610 standards. The stoichiometric Fe content of bornite, chalcopyrite and pyrite were considered as internal standards. Minimum detection limits of the elements varied with the spot laser diameter. Full results and detection limit of elements for each ablated spot are reported in Supplementary Table I.

Each ablation spot represents the measurement results from one mineral grain (crystal) performed in areas without visible solid inclusions. Element concentrations were calculated by selecting relatively flat signals in LA-ICP-MS ablation profiles (Fig. 3A-B). The exceptionally high values (ablation profile spikes, associated with large mineral inclusions underneath the mineral surface), and other outlier values, which were statistically verified using box and whisker plots (Figs. 4; 5), were excluded from the dataset. The results are given in Supplementary Table I.

For statistical calculations, for the same sulfide mineral in the same sample, the majority of measurements returned results below detection limits for an element in a specific sulfide mineral, no mean content value was calculated for that element. If the majority of measurements of an element from a sulfide mineral were above detection limit, then the contents of that element in the measurements with results below detection limit were assumed to be half of detection limit and were used with that value in the calculation of the mean content.

Pearson coefficients (r) are calculated to determinate the correlation relationships between elements for minimum 5 pair numbers and are shown in Supplementary Table IV and V.

RESULTS

Hydrothermal alteration and mineral assemblage types

Transmitted-light and reflected-light microscopy investigation was performed on each sample in order to determine the ore mineral assemblages and their hydrothermal alteration type and the presence of suitable sulfide crystals for LA-ICP-MS analyses. All samples from Roșia Poieni, Bolcana and Colnic show potassic alteration. The porphyritic texture of the rock can be recognized, with the groundmass containing rounded grains of quartz, feldspar and traces of fine-grained biotite (Fig. 2A-B), while plagioclase phenocrysts display various degrees of hydrothermal alteration to potassic feldspars, albite, and epidote. Hornblende phenocrysts are partially replaced by biotite and chlorite. Intensive biotitization is evidenced at Rovina (sample no. ROV02) and Roșia Poieni. At Colnic, incipient sericitization of plagioclase phenocrysts was observed in sample COL06. All samples from Valea Morii, Bucium-Tarnița (ARS03, ARS06, BI07) and two samples from Rovina (ROV04, ROV16) have moderate chloritic alteration overprinting potassic alteration. In these samples, hornblende and biotite phenocrysts are substituted by chlorite. Plagioclase phenocrysts are partially replaced by albite, epidote and calcite. The groundmass contains potassic feldspar, quartz and secondary chlorite, as substitution of disseminated biotite. In all the aforementioned deposits, sulfides are generally finely disseminated in the rock matrix, commonly exhibiting anhedral outlines (Fig. 2C-H). Sulfides also fill sinuous quartz veinlets (sulfides±granular

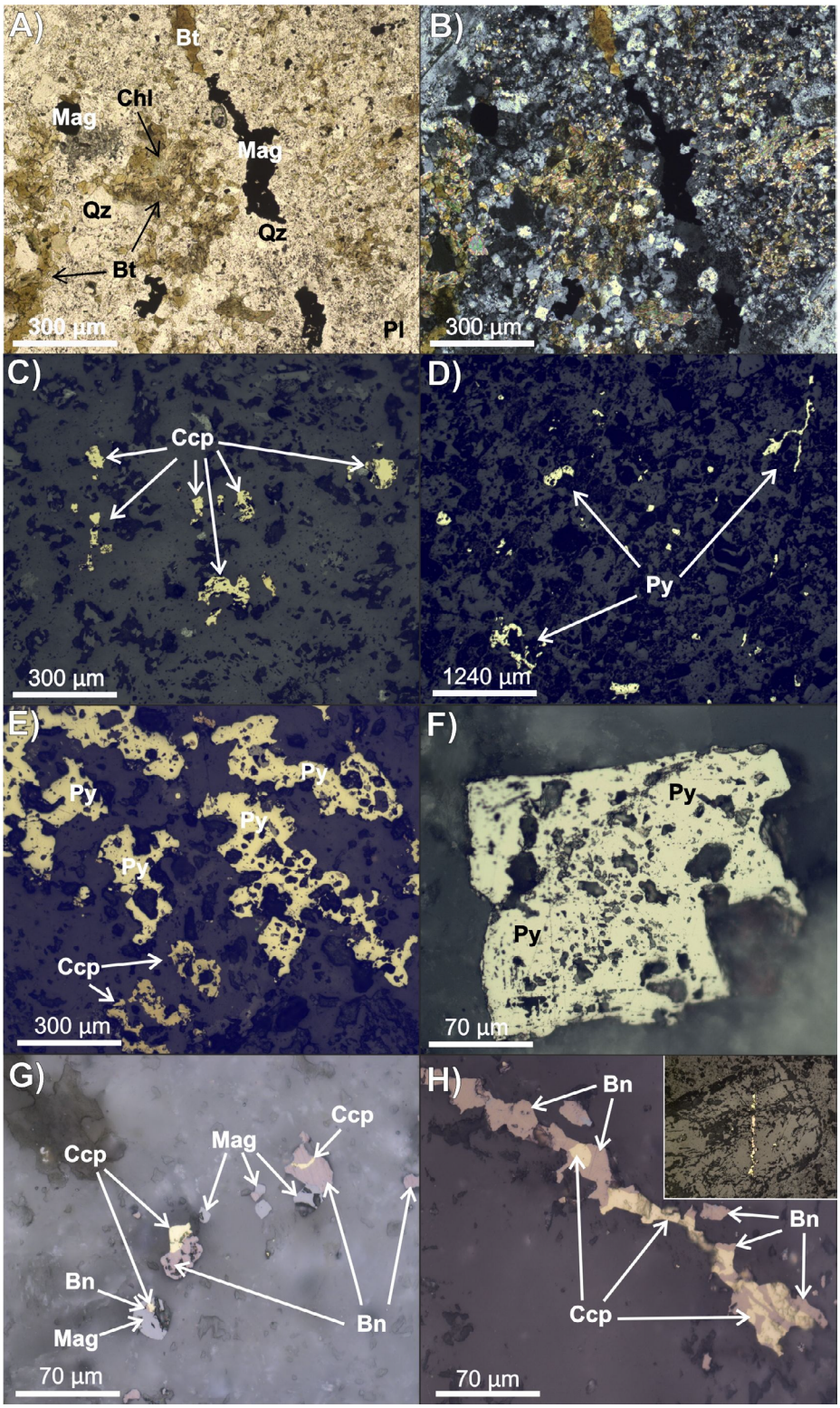

FIGURE 2. Representative images of mineralization and host rock hydrothermal alteration of the studied deposits. A-B) A-type veinlet containing magnetite, rounded quartz crystals, disseminated biotite and weakly altered plagioclase in a potassic altered host rock at Roșia Poieni (RP01; A: plain-polarized transmitted light; B: cross-polarized transmitted light) image. C) Irregularly-shaped chalcopyrite grains in the microdiorite matrix at Valea Morii. D) Irregularly-shaped pyrite grains in the microdiorite matrix at Rovina. In the upper-right corner of the picture, there are millimeter-long microcracks filled by pyrite. E) Irregularly-shaped pyrite and chalcopyrite growths with inclusions of gangue minerals, at Rovina. F) Pyrite subeuhedral crystal with numerous inclusions of gangue minerals, at Colnic. G) Grains of bornite, showing clustering/intergrowths with chalcopyrite and magnetite, at Roșia Poieni. H) Submillimeter-long crack filled with bornite and chalcopyrite, within a plagioclase phenocryst (see inset) at Roșia Poieni. Abreviations (from Warr, 2021): Bt= Biotite, Bn= Bornite, Ccp= Chalcopyrite, Chl= Chlorite, Mag= Magnetite, Py= Pyrite, Pl= Plagioclase, Qz= Quartz.

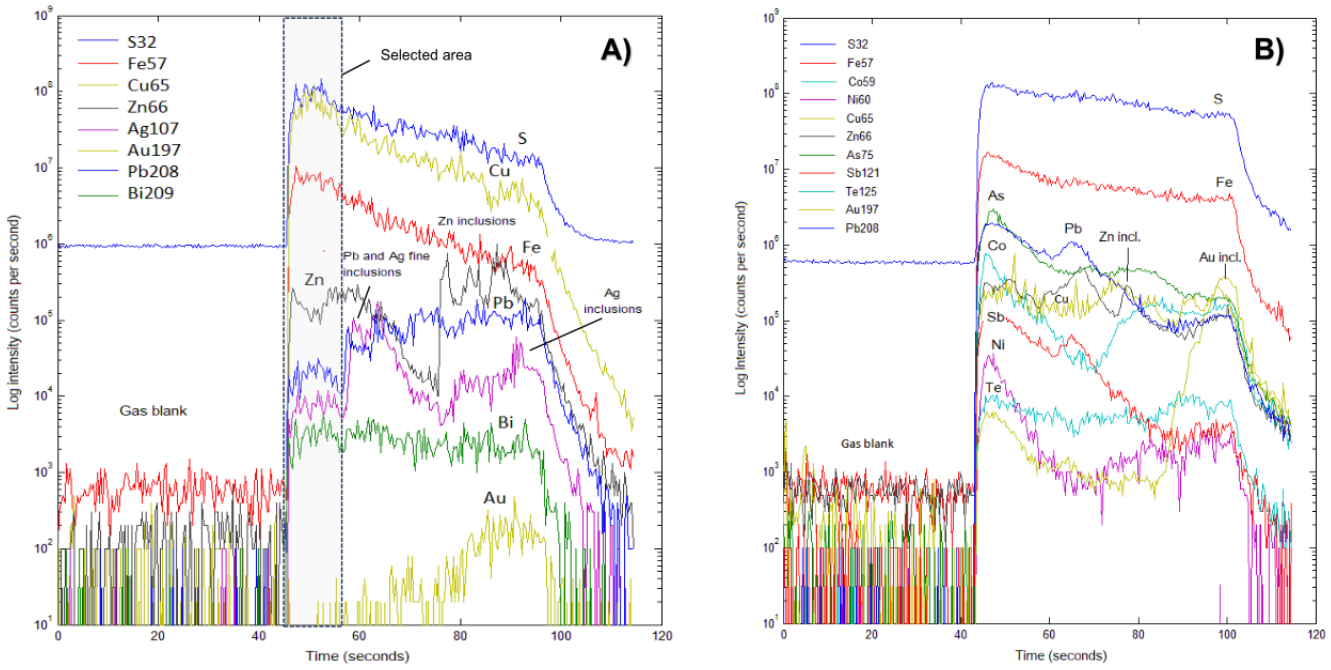

FIGURE 3. Representative LA-ICP-MS downhole profiles of chalcopyrite and pyrite. A) Chalcopyrite with Zn-, Pb- and Ag mineral microinclusions and inhomogeneous Au distribution (Valea Morii- ARS03, spot 13jl11b29). B) Pyrite with inhomogenous distribution of As, Pb, Co, Zn, Sb, Ni and Au. Fine inclusions of Cu-, Zn-, Pb (Sb)- and Au minerals are revealed (Colnic– COL01, spot 13se23b31, excluded from the determination of element concentrations). Gray box from A) represents the selected area used for the element concentrations quantification. Note: In both profiles, the other measured elements display a homogenous distribution. See Table I for corresponding elemental analysis for each spectra (ID number from the brackets).

quartz±magnetite), without alteration hallo, characterized as A-type veinlets in classification of Gustafson and Hunt (1975) and Sillitoe (2010). Chalcopyrite-pyrite-magnetite veinlets and disseminations characterize the Bucium-Tarnița and Valea Morii porphyry-type mineralization. At Bolcana, the chalcopyrite-magnetite±pyrite ore assemblage is well developed in potassic-altered samples, while bornite occurs rarely, as finely disseminated grains, and as inclusions in chalcopyrite and magnetite. Mineralized samples from Colnic consist of disseminated pyrite, and traces of fine-grained chalcopyrite and magnetite. Sulfides usually engulf gangue minerals from the rock matrix (Fig. 2E, F). Bornite and chalcopyrite as fine-grained dissemination and veinlets are dominant at the Roșia Poieni deposit. In this deposit, chalcopyrite-bornite intergrowths were observed in quartz veinlets and microcracks, commonly shorter than 1cm (Fig. 2G, H). Both chalcopyrite and bornite are partially replaced by covellite.

Chemical composition of sulfides and elemental correlation trends

Measured trace element concentration in chalcopyrite, pyrite and bornite grains are shown in Supplementary Table I. Trace element content statistics are provided in Supplementary Table II for chalcopyrite and bornite and in Supplementary Table III for pyrite.

Trace elements in chalcopyrite

The following elements were measured on chalcopyrite crystals: Co, Ni, Zn, As, Se, Ag, Cd, In, Sn, Sb, Te, Au, Tl, Pb and Bi. Most analyses have high dispersion of values around the mean, with a variation coefficient >30%, frequently >100% (Fig. 4; Table II). Several elements yielded results of up to several hundred ppm, with wide ranges of values within each deposit. For example: Zn vary between 42.41±282ppm at Rovina and 273±102 ppm at Bucium-Tarnița, Pb varies between 5.15±7.45ppm at Bucium-Tarnița and 21.88±177ppm at Rovina and Se vary between 277±100ppm at Valea Morii and 403±250ppm at Bolcana. Silver mean values were 1.88±6.36ppm at Bolcana, 8,83±33ppm at Rovina, 27±17.69ppm at Bucium-Tarnița and 24.95±13.88ppm at Valea Morii. In most samples where Ag >100ppm, Ag mimics Pb peaks on LA-ICP-MS transient signals and are not included in this statistic. Tellurium showed concentrations from below the detection limit at Bucium-Tarnița to 12.80±6.01ppm at Bolcana. The highest values are recorded at at Colnic (mean of 36.06ppm). Te-bearing mineral inclusions (*e.g.* Te-Au-Ag and Te-Bi) were identified on the LA-ICP-MS profiles at Bolcana. The Au shows below detection limit values in most of the analysis. Indium mean values range from 2.71±3.39ppm at Valea Morii to 10.10±3.65ppm at Bolcana. Cadmium has the highest mean value at Colnic

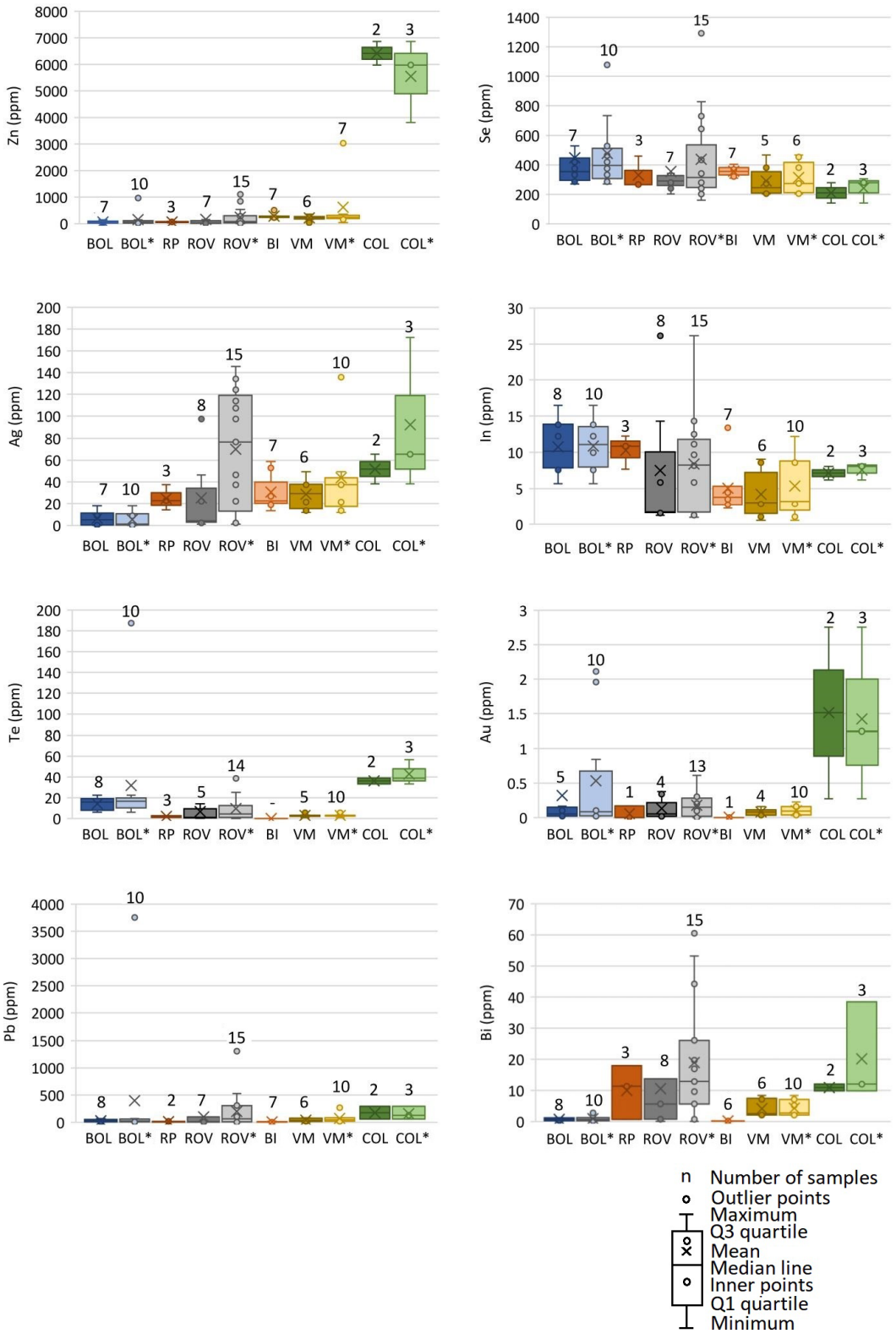

FIGURE 4. Box and whisker plots for selected elements in chalcopyrite. Two data sets are plotted for each deposit: one set with the values for inclusion-free chalcopyrite and the second set with all values, including those with mineral inclusions (*). Legend: BOL= Bolcana (inclusion-free crystals), BOL*= Bolcana (all crystals), RP= Roșia Poieni (all crystals), ROV= Rovina (inclusion-free crystals), ROV*= Rovina (all crystals), BI= Bucium-Tarnița (all crystals), VM= Valea Morii (inclusion-free crystals), VM*= Valea Morii (all crystals), COL= Colnic (inclusion free crystals), COL*= Colnic (all crystals).

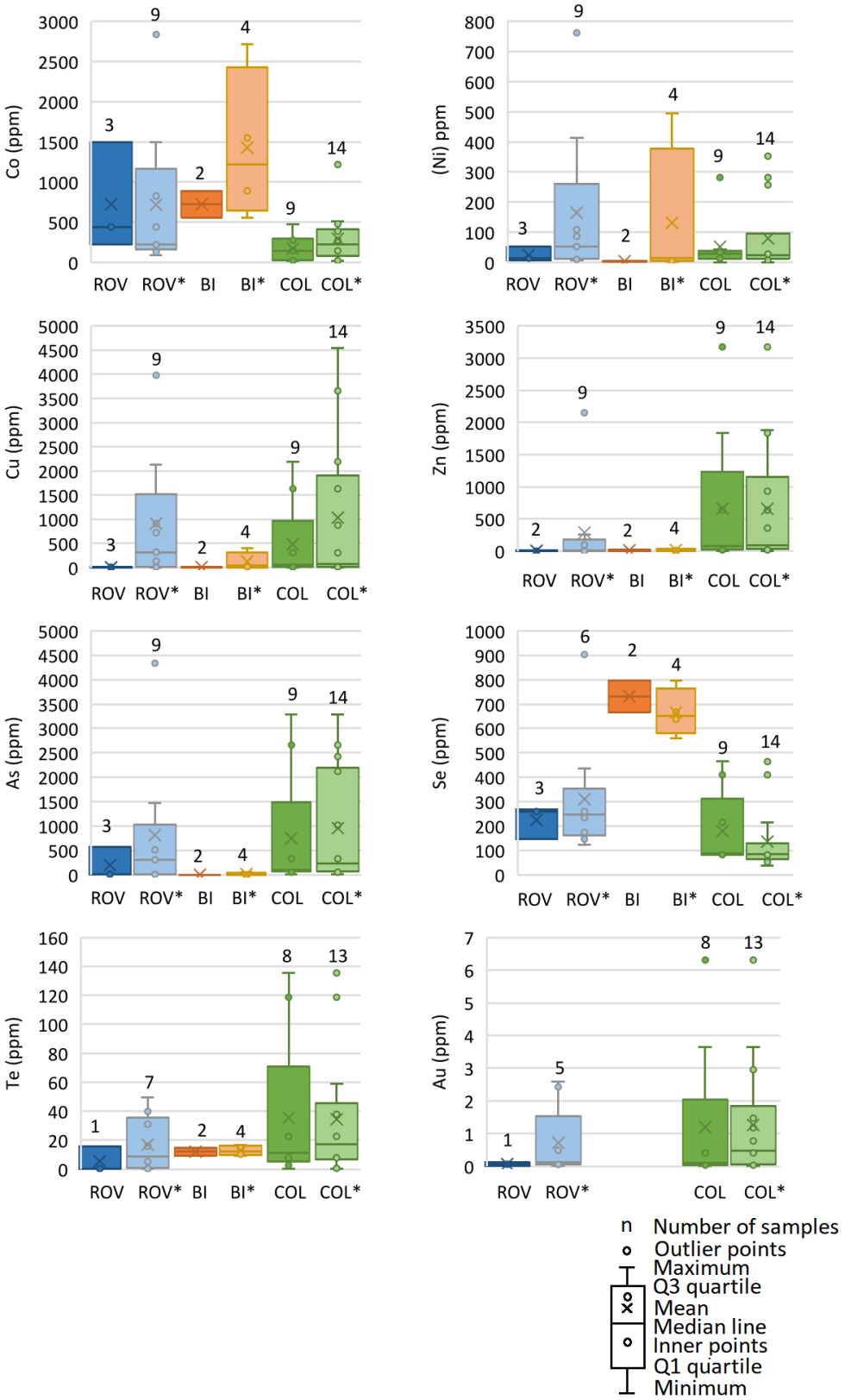

FIGURE 5. Box and whisker plots for selected elements in pyrite. Two data sets are plotted for each deposit: one set with the values for inclusion-free pyrite and the second set with all values, including those with mineral inclusions. Legend: ROV= Rovina (inclusion-free crystals), ROV*= Rovina (all crystals), BI= Bucium-Tarnița (inclusion-free crystals), BI*= Bucium-Tarnița (all crystals), COL= Colnic (inclusion free crystals), COL*= Colnic (all crystals).

(36.82ppm) and mean values between 3.94±16.56ppm and 29.72±11.81ppm in the other deposits. Microinclusions of Cd-minerals in chalcopyrite were distinguished for some samples from Valea Morii, Bucium-Tarnița and Rovina. Cadmium profiles mimic the Zn profiles in many samples.

Pearson correlation coefficients of trace elements in chalcopyrite

A positive correlation between chalcopyrite Te and Pb content is outlined at Rovina and Bolcana. There is no correlation of Au with Ag in any deposit. A week correlation of Au with Te, In and Zn is found at Bolcana (r is between 0.53 and 0.66). In shows a strong correlation (r>0.9) with Zn at Bolcana, Rovina and Bucium-Tarnița. The Se-Cd, Se-In, Se-Te, Se-Bi strong positive correlation (r >60) is revealed at Valea Morii. Ag have positive correlation (r >0.75) with Cd and Bi at Bolcana and Rovina, and also with In and Te at Valea Morii. Copper have negative correlation (r >-0.50) with Zn, In, Au, Te and Pb at Bolcana, with Au and Rovina, and also with Zn, Ag and In at Bucium-Tarnita.

Trace elements in bornite

Bornite was identified in samples from Roșia Poieni and Bolcana with optical microscope. However, the small grain size (often <20μm), and its intergrowth with chalcopyrite, and replacement by covellite, caused difficulties in the selection of bornite crystals for LA-ICP-MS analyses. It resulted in the analysis of only six bornite crystals from Roșia Poieni. The results indicate significant concentrations of Bi, Se, Pb, Ag and Te (Table II). The average Au value is 0.16ppm, with fine gold microinclusions in some bornite grains. LA-ICP-MS spectra from bornite analyses indicated the presence of fine-grained Pb microinclusions.

Trace elements in pyrite

The chemical composition of pyrite was investigated in several samples from Rovina, Bucium-Tarnița, Valea Morii, and Colnic deposits. LA-ICP-MS profiles revealed a grain-scale heterogeneous distribution for many elements (*e.g.* Co, Ni, As, Cu, Zn and Pb; Fig. 3B). Most analyses have high dispersion of values around the mean, with a variation coefficient >30%, frequently >100% (Fig. 5; Table III). Gold was detected in 76 % of the pyrite analyses from all deposits. Gold content of the studied deposits varies from below of detection limit (at Bucium-Tarnița) to 0.17±0.13ppm at Colnic, with mean content of 0.05ppm at Valea Morii and 0.06ppm at Rovina. The highest mean value of As are at Colnic (166ppm). A slightly heterogeneous distribution of As is outlined in several pyrite crystals from Valea Morii, Colnic and Rovina. Cobalt and Ni reach mean values up to 704ppm and 20.64ppm at Bucium-Tarnița and Colnic, respectively. However, individual values could vary by two orders of magnitude within the same deposit and from one deposit to another. Indium has 0.15ppm at Colnic. Copper, Pb, and Zn microinclusions in pyrite, observed on the LA-ICP-MS spectra, were commonly found in all the studied deposits. In most pyrite crystals from the studied deposits where Cu spikes were observed in the LA-ICP-MS profile, it is accompanied with elevated trace element content (*e.g.* Ag, Au, Zn, Pb and Bi). Gold microinclusions were found at Rovina and Colnic (Fig. 3B). The presence of Sn mineral inclusions can be found occasionally in the pyrite from Valea Morii and Colnic, while Ag-bearing minerals inclusions are present at Colnic.

Pearson correlation coefficients of trace elements in pyrite

There is a strong correlation of Au with Te, Ag, Cu and Zn at Colnic (r >0.90) in the free inclusion pyrite. Tellurium is strongly positive correlated with Au, Cu, Pb and As at Colnic (r >0.80). Indium shows a high positive correlation of Zn and Cu (r >0.90).

DISCUSSION

Incorporation of trace elements in pyrite, chalcopyrite and bornite

Time-resolved downhole profiles collected by LA-ICP-MS give a valuable image on the trace elements distribution within the host mineral. Therefore, smooth LA-ICP-MS downhole profiles of analyzed isotopes indicate the presence of micron-scale inclusions below the sample surface, while flat profiles suggest residence (at least partially) in solid solution (Cook *et al.*, 2011 and references therein). Based on the relatively flat shape of the transient signal, it is supposed that trace elements are mostly incorporated as solid solution within the sulfide mineral structure, involving complex substitution mechanisms. It is generally accepted that in chalcopyrite mineral lattice, Cu ions could be direct substituted by Zn^{2+}, but also by In^{3+}, Se^{3+}, Sn^{4+}, Bi^{4+}, coupled with Ag substitution. Similary, Fe is substituted by Co and Ni, and S by Se and Te (Cook *et al.*, 2011; George *et al.*, 2018; Thang *et al.*, 2025). Trace elements in pyrite could occur as lattice substitutions, *e.g.* As, Se for S and Co and Ni for Fe, and also coupled substitution mechanism of the type $Au^{3+}+Cu^{+}\leftrightarrow 2Fe^{2+,}$ and As^{3+} substitutes for Fe^{2+} according to $Ag^{+}+As^{3+}\leftrightarrow 2Fe^{2+}$ (Deditius *et al.*, 2014; Gregory *et al.*, 2015; Keith *et al.*, 2022 and references therein). Arsenic facilitates the incorporation of heavier and larger elements relative to S and Fe in pyrite lattice by structural distortion mechanism (Deditius *et al.*, 2014; Reich *et al.*, 2005). Low As contents in pyrite from studied deposits suggest that heavier and larger elements (*e.g.* Te, Au, Pb) are not only present in solid solution, but also as inclusions

(Keith *et al.*, 2022). Numerous ablated Cu-(Fe) sulfides show spikes in the Pb and Zn transient signals, inferring sub-microscopic Zn- and Pb-bearing mineral inclusions, probably galena and sphalerite (Fig. 3A, B). These were found in the majority of chalcopyrite and pyrite grains from all deposits. Frequently, Pb and Zn presented overlapping of their peaks suggesting sphalerite-galena co-saturation with chalcopyrite (Maydagan *et al.*, 2013). In most samples of chalcopyrite, where Ag >100ppm, Ag mimics Pb peaks on LA-ICP-MS transient signals indicating that a part of Ag is incorporated in some Pb mineral inclusions. The occurrence of Ag-mineral microinclusions in chalcopyrite can be visible on some LA-ICP-MS transient signals signal at Rovina and Valea Morii (Fig. 3A). Gold-bearing microinclusions were identified by LA-ICP-MS transient signals in chalcopyrite from Valea Morii, Colnic, and Bolcana. Some of these Au-bearing inclusions also show elevated content of Ag and Te, suggesting the occurrence of electrum and Au-tellurides microinclusions. Cadmium profiles mimic the Zn profiles in many samples, reflecting the concentration of Cd as a trace element in Zn-bearing mineral inclusions from chalcopyrite. In bornite, LA-ICP-MS spectra analyses indicated the presence of fine-grained Pb microinclusions, probably galena enriched in Bi, Ag, and Zn, as it results from the superposition of their profiles.

In pyrite, the highest values of Cu, Zn and Pb are related to the abundant mineral microinclusions, as inferred from the spiky spectra downhole trace element ablation profiles (Fig. 3B). Occurrence of Co and Ni discrete mineral inclusions within pyrite is possible at Valea Morii and Colnic, as shown in LA-ICP-MS transient signals.

In contrast, downhole trace element ablation profiles that mimic those of the major elements indicate homogeneous substitution into the host crystal lattice but, theoretically these profiles could also result from homogeneously distributed micro- or nanoparticles (100–2500nm and <100nm, respectively) (Cook *et al.*, 2011 and references therein). At the same time, the presence of mineral nanoinclusions can also be deduced from the positive correlation of chemically compatible elements e. g. Bi-Te Au-Te, Au-Ag-Te or Au-Cu-Te (Cook *et al.* 2011; Keith *et al.*, 2017). Based on this consideration, a positive correlation between Te and Pb content in chalcopyrite at Rovina and Bolcana suggests that a part of the Te in these deposits may be related to galena or Pb-telluride nanoinclusions. Similarly, a good correlation of In with Zn at Bolcana, Rovina and Bucium-Tarnița indicates that in these deposits In could be related to Zn-bearing mineral micro- or nano-particle inclusions (probably sphalerite) rather than being trapped in the chalcopyrite mineral lattice. Morover, a positive correlation between Ag and Cd, In, Te and Bi within chalcopyrite could indicate that these elements could be also incorporated into the chalcopyrite lattice through coupled substitution, as described above. Negative correlation between Cu and Zn, In, Te and Au at Bolcana and Bucium–Tarnița confirms a substitution of Cu by these elements in chalcopyrite mineral lattice.

In pyrite, positive correlation of trace elements with geochemical affinity (Table V) suggests that these elements are incorporated in the pyrite mineral lattice in similar conditions (Keith *et al.*, 2018 and references therein).

In previous work, Cioacă *et al.* (2014) suggested that high concentrations of Se, Te, Bi and Ag in Cu minerals (bornite and chalcopyrite) and pyrite, outlined from the EMPA data, may be related to the presence of fine-particle inclusions. This study confirms that Pb, Cu, Au, Ag and Te are trapped both as solid solution and as micro- or-nanoinclusions of minerals in all studied sulfides, as shown on LA-ICP-MS downhole profiles. Pb-mineral inclusions have influence on the concentration and distribution of several elements such as Ag, Au, Zn, Te and Bi, in both chalcopyrite and pyrite, evidenced by the fact that these elements follow Pb peaks on the several LA-ICP-MS downhole profiles in chalcopyrite and also in pyrite from all deposits. This deduction is consistent with the positive correlations between Pb and these elements from pyrite at Colnic, and between Pb and Zn or Te in chalcopyrite from Bolcana and Rovina (Tables IV; V). Galena inclusions from pyrite contain up to 3,700ppm Ag, 27,190ppm Se, 1,500ppm Ge and 780ppm Te, as measured at Colnic, Bolcana and Valea Morii (Cioacă *et al.*, 2014). Several spikes of Cu on pyrite LA-ICP-MS profiles suggests the presence of numerous microinclusions of Cu minerals and sometimes these are mimicked by Pb, Zn, Au, Ag, Bi and Te spikes. In consequence, high content of these elements in some pyrite grains are influenced by the presence of Cu mineral inclusions, which are probably chalcopyrite.

Comparison of trace elements in bornite, chalcopyrite and pyrite

Both chalcopyrite and bornite could incorporate Bi, Au, Ag, Se, Te, Ge, In and Sn (*i.e.* 10s to 1000s ppm) in their crystal lattice in various types of ore deposits, including porphyry copper, skarn, and epithermal veins (Arif and Baker, 2004; Cook *et al.*, 2011; Crespo *et al.*, 2020; George *et al.*, 2018; Kesler *et al.*, 2002; Simon *et al.*, 2000). Similarly, pyrite is known as good host for Au, As, Ni, Co, Te, Ge and Tl (Crespo *et al.*, 2020; Deditius *et al.*, 2014; King *et al.*, 2014; Reich *et al.*, 2005, 2013; Rivas-Romero *et al.*, 2021). Where bornite and chalcopyrite coexist, bornite incorporates significantly more Au than chalcopyrite (Arif and Baker, 2004; Kesler *et al.*, 2002; Simon *et al.*, 2000). Previous EMPA results indicate that bornite and porous pyrite are the best host of gold as Au-bearing mineral inclusions in the porphyry type mineralization of the Metaliferi Mountains

(Cioacă *et al.*, 2014). Our LA-ICP-MS results revealed low concentrations of Au in both bornite (mean value 0.16ppm) and chalcopyrite (below detection limit) at Roșia Poieni. Other elements, such as Ag, Te, Se and Bi are enriched in bornite compared to chalcopyrite. An opposite tendency is shown by Co, Zn, Sb, In and Cd, which are preferentially concentrated in chalcopyrite rather than in bornite (Table II). This tendency was also reported from other porphyry copper deposits, such as Batu Hijau, Indonesia (Arif and Baker, 2004), Elatsite, Bulgaria (Cook *et al.*, 2011; George *et al.*, 2018) and Río Blanco, Chile (Crespo *et al.*, 2020). Generally, in the investigated samples, when chalcopyrite and pyrite coexist, chalcopyrite is a better host for Zn, Se, Ag, In, Sn, Te, Au, Pb and Bi, whereas pyrite is a better host for Co, Ni and As. This geochemical pattern has been also observed in other porphyry Cu deposits, such as: Altar, Argentina (Maydagan *et al.*, 2014), Chuquicamata, Chile (Rivas-Romero *et al.*, 2021) and Río Blanco, Chile (Crespo *et al.*, 2020). Exceptions to this geochemical feature occur at Bucium-Tarnița and Colnic, where Te, Se and Bi are preferentially concentrated in pyrite. Comparing our LA-ICP-MS data with previously published EMPA data (Cioacă *et al.*, 2014), we noticed that Au content in sulfides mineral lattice is generally lower than Au content in bulk rock samples from almost all investigated deposits. This suggests that most of the gold detected in bulk rock geochemistry occurs as Au-bearing micro/nano mineral crystals, in sulfides and as free gold in the mass of host rocks, rather than in the crystal lattice of sulfides. LA-ICP-MS profiles confirmed the presence of native gold, electrum, and Au-Ag tellurides in chalcopyrite, pyrite and bornite from all deposits.

Genetic significance of trace elements concentration and distribution within the main sulfides

Application of trace elements ratios in Cu-Fe sulfides

Concentration of trace elements in sulfides is strongly dependent on physico-chemical characteristics of ore forming fluids (Deditius *et al.*, 2014; Gregory *et al.*, 2013; Keith *et al.*, 2018, 2022; Kesler *et al.*, 2002; Maydagan *et al.*, 2013; Reich *et al.*, 2013; Rivas-Romero *et al.*, 2021). Therefore, trace element signatures of sulfides could be used to reconstitute the physico-chemical conditions that were responsible for mineralization and for hydrothermal alteration in hydrothermal systems.

In the investigated porphyry Cu-Au deposits from Metaliferi Mountains, the highest concentrations of Au and Cu are found in the inner zone of the deposits, affected by potassic alteration (Borcoș *et al.*, 1998; Milu *et al.*, 2004; Cioacă *et al.*, 2014), where the deduced temperature of porphyry type mineralization ranges between 310°C and 500°C at Valea Morii (André-Mayer *et al.*, 2001), 400°–600°C at Roșia Poieni (Milu *et al.*, 2004), and from 400°C to more than 600°C at Bolcana (Cioacă, 2011). Experimental data revealed that gold content in copper minerals reflects the phase equilibria in the Cu-Fe-S-O system during cooling, decreasing about one order of magnitude for each 200°C (Simon *et al.*, 2000). Accordingly, the gold amount can reach more than 10ppm in bornite and 1ppm in chalcopyrite at 300°C, if the hydrothermal solutions are saturated in respect with native gold. Considering this, the low Au concentration in bornite and chalcopyrite (<0.2ppm) at Bolcana and Roșia Poieni, where bornite and chalcopyrite coexist could suggest that significant amounts of gold were expelled from the lattice of copper minerals as effect of the changes in host crystal lattice, which becomes more ordered at low temperature, and nucleate as nano- or microparticles (Aird *et al.*, 2021; Cook *et al.*, 2011; Reich *et al.*, 2013; Simon *et al.*, 2000). Alternatively, Au may be preferentially deposited from the beginning as co-precipitated mineral species (*e.g.* native gold, electrum, and Au-Ag tellurides). Based on the frequent detection of gold micro-nanoparticles, we infer that part of the available gold was expelled from the lattice during cooling or during low temperature alteration superimposed on the potassic alteration and occurs as free Au microparticles and other Au-bearing minerals close to Cu minerals similar to other porphyry copper deposits (*e.g.* Batu Hijau, Arif *et al.*, 2004; Pebble, Gregory *et al.*, 2013; Ann-Mason, Aird *et al.*, 2021).

Not only Au concentration in Cu-Fe sulfides is likely temperature-dependent. In general, chalcopyrite related to potassic alteration is enriched in Se, In, Sn, W and Pb with respect to chalcopyrite related to quartz-sericite (phyllic) and chloritic (propylitic) alteration types (Rivas-Romero *et al.*, 2021). Based on these observations in the study of Chuquicamata Underground Mine porphyry Cu-Mo deposit, Rivas-Romero *et al.* (2021) used several elemental ratios to discriminate between high temperature and low temperature mineral assemblages in porphyry copper deposits, *e.g.* In/Se in chalcopyrite, and Co/Ni, Ag/Co and Co/Cu in pyrite. The authors concluded that the lowest In/Se ratios (~0.001) in chalcopyrite are related to early stage of potassic alteration, defined by the authors as background potassic alteration which is characterized by abundant secondary biotite, potassic feldspar, albite, and minor calcite. The mineralization occurs as disseminations and to a lesser extent, as irregular "A-type" quartz-bearing micro-veinlets comprising mainly chalcopyrite, with bornite and pyrite occurring only locally. Values around 0.01 of In/Se ratio characterize the chalcopyrite from intense potassic alteration zone, while values ranging between 0.01 and 1 characterize the chloritic and quartz-sericite alteration zones. The intense potassic alteration in Chuquicamata Underground Mine is characterized by the presence of microbreccia with a fine matrix of

micro- to crypto-crystalline quartz and K-feldspar. The mineralization consists of two types of micro-veinlets with bornite±digenite±covellite or chalcopyrite±bornite±covellite±digenite, and also two types of continuous cm-thick veinlets: chalcopyrite veinlets and quartz±molybdenite "B-type" veinlets. Chloritic alteration predominates with the selective chloritization of mafic minerals and micro-veinlets of calcite, ankerite, and hematite and associated mineralization corresponds mainly to pyrite with minor chalcopyrite (Rivas-Romero *et al.* (2021). In the investigated deposits from Metaliferi Mountains, the In/Se ratio in chalcopyrite from samples with potassic alteration at Bolcana, Roșia Poieni and Colnic, having similar characteristics with early stage potassic alteration zone from Chuquicamata Underground Mine, vary between 0.01 and 0.04, ranged close to the chloritic or sericitic alteration zones. At Rovina, Bucium-Tarnița and Valea Morii, where chloritic-sericitic alteration overprints the potassic zone In/Se ratio varies between 0.01 and 0.02 (Fig. 6A; Table II). Also, low values of the In/Se ratio in chalcopyrite, where the presence of sphalerite and galena inclusions is common, may also be caused by a preferential distribution of these elements in the mineral lattice of these inclusions, rather than as solid solution in chalcopyrite. In this case, the In/Se ratio becomes irrelevant in the appreciation of the relative temperature conditions of the mineralization in relationship to the associated hydrothermal alteration.

Trace element ratios in pyrite

Many studies have documented the use of Co/Ni ratios in pyrite as indicator of the physicochemical conditions during pyrite precipitation (*e.g.* Bajwah *et al.*, 1987; Bralia *et al.*, 1979; Brill, 1989; Corral *et al.*, 2016; Crespo *et al.*, 2020; Fintor *et al.*, 2011; Goldschmidt, 1954; Keith *et al.*, 2022; Loftus-Hills and Solomon, 1967; Raymond, 1996), suggesting that Co/Ni <1 is indicative of low temperature of precipitation (*e.g.* sedimentary) while higher values are indicative of hydrothermal deposits (Co/Ni= 5-10) or magmatic sources (Co/Ni>10). In our study area, almost all Co/Ni ratios in pyrite are greater than 1 (Fig. 6B), most of these being higher than 10, which suggests a genetic relation with high-temperature magmatic-hydrothermal processes (*e.g.* Bralia *et al.*, 1979; Koglin *et al.*, 2010; Keith *et al.*, 2022; Sykora *et al.*, 2018). When high Co/Ni ratios are associated with high contents of Ni and Co (measurable in weight percents), a mafic magmatic source is supposed to have been involved in the formation of the ore (del Real *et al.*, 2020; Naglik *et al.*, 2022; Reich *et al.*, 2017). The pyrite crystals studied here, show Co contents up to several hundreds ppm and only one measurement with 0.15% Co, while Ni contents are less than 100ppm, with a single value close to 300ppm. To outline the influence of mineral inclusions on the values of the elemental ratio, we plotted the values of both inclusions free pyrite

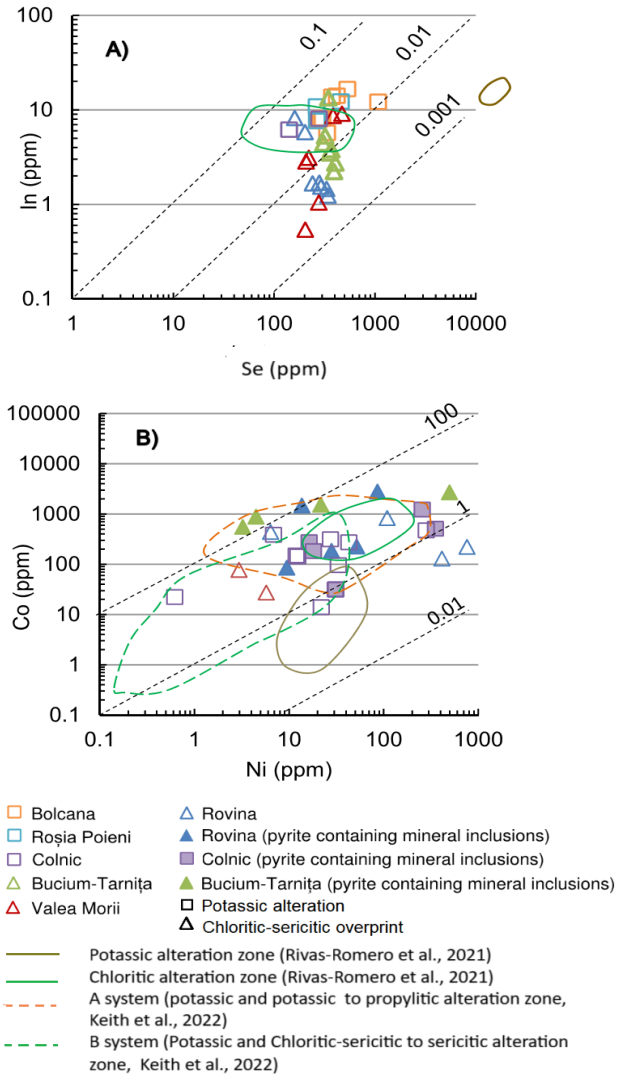

FIGURE 6. Elemental concentration scatterplots for chalcopyrite and pyrite. A) In versus Se in chalcopyrite. B) Co versus Ni in pyrite.

and the pyrite containing discrete mineral inclusions on discriminatory elemental ratio scatterplots. In general, the values of both populations are placed in the same values ranges. Comparing our data with the ones from other porphyry Cu deposits (Fig. 6B) most samples are placed in the potassic alteration field from Koloula porphyry Cu-Au deposit (Keith *et al.*, 2022), but several samples from Colnic and Rovina also are placed in the choritic zone from Chuquicamata Underground Mine (Rivas Romero *et al.*, 2021).

Another elemental ratio that could be useful as a tool for evaluation of porphyry system evolution is based on Ag/Co ratio vs Co/Cu ratio in pyrite (Rivas Romero *et al.*, 2021). Interpreting the analyzed data on pyrite geochemistry from different hydrothermal alteration zones in the Chuquicamata Underground Mine, the authors identified

that the Ag/Co ratio increases from the chloritic zone to the potassic zone, ranging from ~0.001 to 10, while the Co/Cu ratios decrease from ~100 to 0.001 from the chloritic to background potassic alteration. Intermediate ratios are related to the pyrite from the quartz-sericite alteration. Our study shows at Rovina and Bucium-Tarnița, where chloritic-sericitic alteration overprints the potassic zone, Ag/Co ratio is ~0.001 and Co/Cu ratio >1 (0.7-398) in pyrite suggest precipitation at low temperature (Table III; Fig. 7A). At Colnic, Ag/Co <0.02, and Co/Cu ratio vary between 0.1 and 28, respectively. These values are characteristic of low temperature pyrite from chloritic/quartz-sericitic zones, respectively (Fig. 7A).

Another study on the use of pyrite geochemistry in interpreting the evolution of a Cu-Au porphyry system,

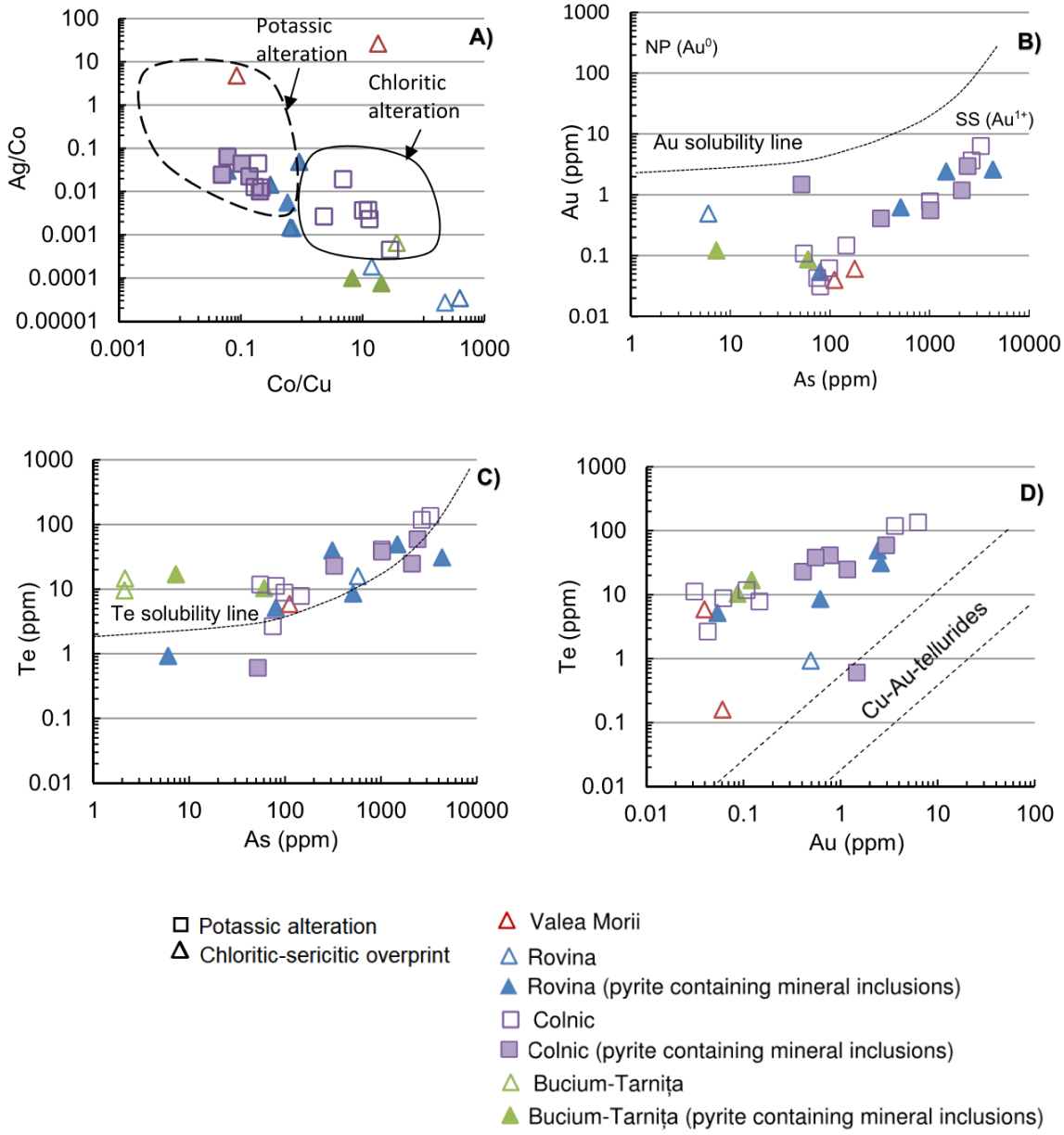

FIGURE 7. Elemental concentration scatterplots for pyrite. A) Ag/Co versus Co/Cu ratio in pyrite. Delimited areas represent the corresponding potassic and chloritic areas for Chuquicamata Underground deposit (from Rivas-Romero *et al.*, 2021). B) Concentration of Au versus As in pyrite. Dashed line represents the gold solubility line in As-rich pyrite from Reich *et al.* (2013). C) Plot of Te versus As concentrations in pyrite. Dashed line represents the Te solubility line in pyrite from Keith *et al.* (2018). Tellurium concentrations above the solubility line indicate the occurrence of telluride inclusions. D) Plot of Te versus Au concentrations. Dashed line represents the Te-Au ratio compositional range of common Cu-Au-tellurides based on their Te/Au ratio, from Keith *et al.* (2018). Note that measured data corresponding to the pyrite containing large mineral inclusions are marked individually, in order to highlight the influence of the detected microinclusions on the concentrations of the plotted elements in pyrite.

concludes that trace element ratios in pyrite show systematic variations with fluid temperature and salinity, phase separation and mixing of magmatic fluids and meteoric waters (Keith *et al.*, 2022). The authors investigated Cu-Au Koloula porphyry-epithermal system from Solomon Islands and concluded that the mineralization in the potassic alteration zone, which is deposited at temperatures of up to 700ºC, from hypersaline liquid magma-derived fluid, and lithostatic pressure, it is characterized by following geochemical features of pyrite: Se/Ge ~100, Se/Te >50, Co/As >1 and Co/Ni >50. Transition to the chlorite-sericite to sericitic alteration zone, developed in boiling conditions, is characterized by Se/Ge <100, Se/Te <50, Co/As <1 and Co/Ni >50 ratios in pyrite. Shallowest part of the mineralization from the epithermal transition zone precipitated from vapor-rich fluids that condensed into meteoric waters and pyrite record Se/Ge <100, Se/Te <50, Co/As <1 and Co/Ni <50. Reffering to the geochemical pattern of porphyry-epithermal system proposed by Keith *et al.* (2022), both Rovina and Bucium-Tarnita could indicate high temperature and hypersaline magma derived mineralizing fluids and supercritical conditions (Co/Ni >50, Co/As >1 and Se/Te >50), related to potassic alteration zone. In this case, the few values with Co/Ni ratio less than 10 at Rovina and Bucium-Tarnița might have been (re)crystallized under the P-T conditions of chloritic-sericitic alteration that partially overprinted the potassic alteration zone. Irregularly-shaped pyrite and chalcopyrite growths with inclusions of gangue minerals (Fig. 2D, E) could by explained as rapid crystallization as effect of changes in fluid composition caused by fluid mixing and repeated and intermittent pulses of magmatic fluids rather than significant changes of P-T conditions.

At Valea Morii and Colnic, values of Co/As <1, Co/Ni <50 and Se/Te ratio <50 in pyrite suggest that mineralization from these deposits precipitated from vapor-rich fluids, mixed with meteoric water and under hydrostatic pressure. This is also supported by the anhedral morphology and porous texture of the pyrite crystals (Fig. 2F), which suggest rapid precipitation as effect of fluid boiling at hydrostatic pressure conditions.

This is also envisaged in the heterogeneous distribution of Au content in sulfides. In this study, we found Au in lower concentrations in the pyrite mineral lattice, with highest values related to Au-bearing mineral microinclusions (Table I; Figs. 4; 5). Additionally, pyrite contains trace elements (*e.g.* Co, Ni, Cu, Zn, As, Se, Te, Bi), which favored Au concentration in the crystal lattice. Gold trapping in pyrite lattice presumably was favored by the presence of other trace elements, such as As, Cu, Co or Te that caused the deformation of the pyrite structure (Deditius *et al.*, 2014; King *et al.*, 2014; Reich *et al.*, 2005 and references there in). Gold may also be incorporated in pyrite through the adsorption of Au-sulfide complexes onto the surface of the As-rich, Fe-deficient pyrite, during rapid growth under non-equilibrium conditions (Deditius *et al.*, 2014; King *et al.*, 2014; Reich *et al.*, 2005). High positive correlation values of Au with Cu, Co and As in pyrite from Colnic (Table V), suggest that these elements triggered the incorporation of Au in pyrite. However, pyrite from the investigated deposits contains more Te than Au, with a high positive correlation between Au and Te at Colnic (Table V) suggesting that Te can facilitate Au capture in pyrite lattice (Keith *et al.*, 2018). Our data indicate that pyrite analyses with detected Au are clustered in the Au solid solution field of the Au-As plot (Fig. 7B). Previously, Cioacă *et al.* (2014) found that Au in pyrite crystals is also present as nanoparticles, therefore, in the studied porphyry copper deposits. Au is present in pyrite both as solid solution and as gold nanoparticles. This fact is considered to be related to the evolution of hydrothermal fluids transitioning from undersaturation to supersaturation dominant state of native Au for high-temperature mineralizing fluids (Deditius *et al.*, 2014 and references therein). Similarly to Au, Te solubility limit in pyrite lattice is a function of As content (Keith *et al.*, 2018). The plots of our data on Te-As and Te-Au diagrams (Fig. 7 C, D) suggest that Te dominantly occurs as micron to sub-micron sized Au-Te, Au-Ag-Te, or Au-Cu-Te bearing minerals, similar to the situation presented by Keith *et al.* (2018). At the crystal-scale, the heterogeneous distribution of trace elements in pyrite can be explained by changes in the physico-chemical parameters of mineralizing fluids during mineral growing and/or recrystallization (Gregory *et al.*, 2013; Keith *et al.*, 2018; Reich *et al.*, 2013).

LA-ICP-MS profiles show a slightly heterogeneous/zonal distribution of As, Co, Ni, Cu, Bi, Pb and Zn in most pyrite crystals (Fig. 3B), while microscope study shows a porous texture of pyrite from all deposits (Fig. 2E, F). These changes could be interpreted as the result of multiple boiling events that were recognized at Valea Morii, Bolcana, Bucium-Tarnița and Roșia Poieni (André-Mayer *et al.*, 2001; Cioacă, 2011; Dénes *et al.*, 2014; Pintea, 2001; Pettke *et al.*, 2001). Boiling events imply a strong and rapid fluid decompression affecting the metal concentrations by selective partition of metals between coexisting brine (Fe, Zn, Ag, Pb, Tl) and vapors (Cu, As, Au) and causing chemical variations and/or zonations in precipitated minerals (Keith *et al.*, 2018; Pettke *et al.*, 2001). At Colnic, pyrite is associated with A type veins as well as disseminated in potassic-altered host rock, being enriched in Cu, Au, As, Te and Zn, and depleted in Co, Ni and Se as compared to Rovina, Valea Morii and Bucium-Tarnița. This geochemical feature may be explained by mixing processes between magmatic vapors and hydrothermal fluids. They can induce the intermittent supersaturation of Cu in the hydrothermal fluid and the nucleation of chalcopyrite micro- to nanoparticles at or close to the pyrite–fluid surface (Reich *et al.*, 2013).

CONCLUSIONS

Our research revealed that chalcopyrite, bornite and pyrite from the studied porphyry Cu-Au deposits of the Metaliferi Mountains contain elevated concentrations of precious metals (Ag-Au) as well as other metals and metalloids (*e.g.* Pb, Zn, Cu, In, Cd, Co, As, Te, Bi and Se). These elements occur as solid solution, and as micro- or nano-inclusions in sulfides, as well.

In bornite-chalcopyrite mineral assemblages related to potassic alteration, chalcophile elements (*e.g.* Ag, Bi, Se and Te) are preferentially concentrated in bornite compared to chalcopyrite, occurring in the range of tens to hundreds ppm in inclusion-free crystals. In chalcopyrite-pyrite-magnetite and pyrite-chalcopyrite mineral assemblages related to both potassic and potassic with chloritic-sericitic overprint alteration, chalcopyrite concentrates most Au, Ag, Pb, Zn and In, while pyrite is the main host of Co, Ni and As. Other elements, such as Te, Se and Bi reach variable amounts in both pyrite and chalcopyrite in all deposits, with highest Se and Te contents in pyrite from samples of chlorite-sericite (propylitic) alteration zones from Bucium-Tarnița deposit.

The mean Au content in sulfides is generally lower than Au content in bulk rock samples, indicating that only part of gold is present as trace element in sulfides, the rest occurring as free gold. Au and Te are mostly related to Cu-, Au- and Te-bearing micro- or nano-inclusions.

The trace element ratios in sulfides are in agreement with the variability in the physico-chemical conditions during precipitation and with the overlapping of late, low-temperature, alteration on the potassic alteration. In these conditions, the Se/In ratio in chalcopyrite and Co/Ni, and Ag/Co vs Co/Cu ratios in pyrite are not useful to differentiate the chlorite-sericite (propylitic) and potassic rich zones in the porphyry copper systems studied here.

ACKNOWLEDGMENTS

The authors thank the mining company SAMAX Romania SRL for their support during fieldwork and sample collection in 2011. M.E. Călugăru (Cioacă) is grateful to Professor Cristoph Heinrich from Institute of Geochemistry and Petrology, ETH Zurich (Switzerland) for the assistance with LA-ICP-MS analyses. The journal reviewers Alexandre Cugerone and Carlos Jimenes are thanked for constructive comments that improved the quality of the manuscript. On the part of Geologica Acta, Isaac Corral is thanked for efficient editorial handling.

FUNDING

This work was supported by a grant of the Romanian National Authority for Scientific Research (ANCS-UEFISCDI), under Grant number PN-II-RU-PD-2011-3-0172.

REFERENCES

Aird, H.M., Purcell, C.K., DeWitt, N., Matthews, J., Capurro, T., Claiborne, J., Bermudez, J., Meisel, Z., 2021. Gold- and silver-bearing assemblages in the Ann-Mason copper porphyry deposit, Yerington, Nevada. Ore Geology Reviews, 138, 104339. DOI: https://doi.org/10.1016/j.oregeorev.2021.104339

André-Mayer, A.S., Leroy, J.L., Marcoux, E., Lerouge, C., 2001. Inclusions fluides et isotopes du soufre du gisement Cu–Au de Valea Morii (Monts Apuseni, Roumanie): un télescopage porphyre–épithermal neutre. Earth and Planetary Science Letters, 333, 121-128. DOI: https://doi.org/10.1016/S1251-8050(01)01611-1

Arif, J., Baker, T., 2004. Gold paragenesis and chemistry at Batu Hijau, Indonesia: implications for gold-rich porphyry copper deposits. Mineralium Deposita, 39, 523-535. DOI: https://doi.org/10.1007/s00126-004-0433-0

Bajwah, Z.U., Seccombe, P.K., Offler, R., 1987. Trace element distribution Co: Ni ratios and genesis of the Big Cadia iron-copper deposit, New South Wales, Australia. Miner. Deposita 22, 292-300.

Blannin, R., Frenzel, M., Tușa, L., Birtel, S., Ivășcanu, P., Baker, T., Gutzmer, J., 2021. Uncertainties in quantitative mineralogical studies using scanning microscope-based image analysis. Minerals Engineering, 167, 106836. DOI: https://doi.org/10.1016/j.mineng.2021.106836

Borcoş, M., Vlad, S., Udubaşa, G., Găbudeanu, B., 1998. Qualitative and quantitative metallogenetic analysis of the ore genetic units in Romania. Romanian Journal of Mineral Deposits, 7, 1-160.

Bralia, A., Sabatini, G., Troja, F., 1979. A revaluation of the Co/Ni ratio in pyrite as geochemical tool in ore genesis problems. Mineralium Deposita, 14, 353-374.

Brill, B.A., 1989. Trace-element contents and partitioning of elements in ore minerals from the CSA Cu-Pb-Zn deposit, Australia, and implications for ore genesis. Canadian Mineralogist, 27, 263-274.

Brodbeck, M., McClenaghan, S.H., Kamber, B.S., Redmon, P.B., 2022. Metal(loid) Deportment in Sulfides from the High-Grade Core of the Bingham Canyon Porphyry Cu-Mo-Au Deposit, Utah. Economic Geology, 117(7), 1521-1542. DOI: https://doi.org/10.5382/econgeo.4954

Cheşu, M., 1983. Minor elements in non-ferrous ores from Romania. Bucharest, Editura Tehnică. (in Romanian).

Cioacă, M.E., 2011. Fluid evolution in the Bolcana ore deposit, Metaliferi Mountains (Romania). Carpathian Journal of Earth and Environmental Sciences, 6, 215-224.

Cioacă, M.E., Munteanu, M., Qi, L., Costin, G., 2014. Trace elements concentration in porphyry copper deposits from Metaliferi Mountains, Romania. A reconnaissance study. Ore Geology Reviews, 63, 22-39. DOI: https://doi.org/10.1016/j.oregeorev.2014.04.016

Cook, N.J., Ciobanu, C.L., Danyushevsky, L.V., Gilbert, S., 2011. Minor and trace elements in bornite and associated Cu–(Fe)-sulfides: LA-ICP-MS study. Geochimica et Cosmochimica Acta, 75, 6473-6496. DOI: 10.1016/j.gca.2011.08.021

Corral, I., Cardellach, E., Corbella, M., Canals, À., Gómez-Gras, D., Griera, A., Cosca, M.A., 2016. Cerro Quema (Azuero Peninsula, Panama): Geology, alteration, mineralization, and geochronology of a volcanic dome-hosted high-sulfidation Au-Cu deposit. Econonomic Geololy, 111, 287-310. DOI: https://doi.org/10.2113/econgeo.111.2.287

Crespo, J., Reich, M., Barra, F., Verdugo, J.J., Martínez, C., Leisen, M., Romero, R., Morata, D., Marquardt, C., 2020. Occurrence and Distribution of Silver in the World-Class Río Blanco Porphyry Cu-Mo Deposit, Central Chile. Economic Geology, 115(8), 1619-1644. DOI: https://doi.org/10.5382/econgeo.4778

Deditius, A.P., Reich, M., Kesler, S.E., Utsunomiya, S., Chryssoulis, S.L., Walshe, J., Ewing, R.C., 2014. The coupled geochemistry of Au and As in pyrite from hydrothermal ore deposits. Geochimica et Cosmochimica Acta, 140, 644–670. https://doi.org/10.1016/j.gca.2014.05.045.

del Real, I., Thompson, J.F.H., Simon, A.C., Reich, M., 2020. Geochemical and Isotopic Signature of Pyrite as a Proxy for Fluid Source and Evolution in the Candelaria-Punta del Cobre Iron Oxide Copper-Gold District, Chile. Economic Geology, 115(7), 1493-1518. DOI: 10.5382/econgeo.4765

Dénes, R., Marton, I., Kiss, G.B., Ivășcanu, P., Veress, Z., 2014. Additional data regarding the petrography and geochemistry of the magmatic phases and hydrothermal vein types from Bolcana porphyry Cu-Au mineralization (Apuseni Mts., Romania). Romanian Journal of Mineral Deposits, 87(1), 99-104.

Desautels, P., Zurowski, G., Lincoln, N., 2022. Preliminary Economic Assessment, NI 43-101 Tehnical report for Rovina Valley Project. Last accessed: Website: https://www.eurosunmining.com/wp-content/uploads/2021/09/Rovina-Technical-report-February-20-2019.pdf

Fintor, K., Tóth, T.M., Schubert, F., 2011. Hydrothermal palaeofluid circulation in the fracture network of the Baksa Gneiss Complex of SW Pannonian Basin, Hungary. Geofluids, 11, 144-165. DOI: https://doi.org/10.1111/j.1468-8123.2011.00327.x

George. L., Cook, N.J., Crowe, B.B.P., Ciobanu, C.L., 2018. Trace elements in hydrothermal chalcopyrite. Mineralogical Magazine, 82(1), 59-88. DOI: https://doi.org/10.1180/minmag.2017.081.021

Goldschmidt, V.M., 1954. Geochemistry. Oxford, Clarendon Press, 730pp.

Gregory, M.J., Lang, J.R., Gilbert, S., Hoal, K.O., 2013. Geometallurgy of the Pebble Porphyry Copper-Gold-Molybdenum Deposit, Alaska: Implications for Gold Distribution and Paragenesis. Economic Geology, 108, 463-482. DOI: 10.2113/econgeo.108.3.463

Guillong, M., Meier, D., Allan, M., Heinrich, C., Yardley, B., 2008. SILLS: a MATLAB-based program for the reduction of laser ablation ICP-MS data of homogeneous materials and inclusions. In: Sylvester, P. (ed.). Laser Ablation ICP–MS in the Earth Sciences: Current Practices and Outstanding Issues. Vancouver, Mineralogical Association of Canada, Short Course Series, 328-333.

Gustafson, B., L., Hunt, J.P., 1975. The porphyry copper deposit at El Salvador, Chile, 70(5), 857-912. DOI: https://doi.org/10.2113/gsecongeo.70.5.857

Halga, S., Ruff R., Stefanini, B., Nicolici, A., 2010. The Rovina Valley Project, Apuseni Mts., Romania. Gold copper porphyry discoveries in a historic mining district. Romanian Journal of Mineral Deposits, 84, 12-15.

Harris, C.R., Pettke, T., Heinrich, C.A., Roșu, E., Woodland, S., Fry, B., 2013. Tethyan mantle metasomatism creates subduction geochemical signatures in non-arc Cu–Au–Te mineralizing magmas, Apuseni Mountains (Romania). Earth and Planetary Science Letters, 366, 122-136. DOI: 10.1016/j.epsl.2013.01.035

Keith, M., Smith, D.J., Jenkin, G.R.T., Holwell, D.A., Dye, M.D., 2018. A review of Te and Se systematics in hydrothermal pyrite from precious metal deposits: insights into ore-forming processes. Ore Geology Reviews, 96, 269-282. DOI: http://dx.doi.org/10.1016/j.oregeorev.2017.07.023

Keith, M., Haase, M.K., Kivas, A.R., Klemd, R., 2022. Phase separation and fluid mixing revealed by trace element signatures in pyrite from porphyry systems. Geochimica et Cosmochimica Acta, 329, 185-205.

Kesler, S.E., Chryssoulis, S.L., Simon, G., 2002. Gold in porphyry copper deposits: its abundance and fate. Ore Geology Reviews, 21, 103-124. DOI: https://doi.org/10.1016/S0169-1368(02)00084-7

King, J., Williams-Jones, A.E., Van Hinsberg, V., Williams-Jones, G., 2014. High-Sulfidation Epithermal Pyrite-Hosted Au (Ag-Cu) Ore Formation by Condensed Magmatic Vapors on Sangihe Island, Indonesia. Economic Geology, 109, 1705-1733. DOI: https://doi.org/10.2113/econgeo.109.6.1705

Koglin, N., Frimmel, H.E., Lawrie Minter, W.E., Brätz, H., 2010. Trace-element characteristics of different pyrite types in Mesoarchaean to Palaeoproterozoic placer deposits. Miner Deposita, 45, 259-280. DOI: 10.1007/s00126-009-0272-0

Kouzmanov, K., Pettke T., Heinrich, C.A., Riemer, S., Ivascanu P.M., Rosu, E., 2003. The porphyry to epithermal transition in a magmatic-hydrothermal system: Valea Morii copper-gold deposit, Apuseni Mts, Romania. In: Proceedings to the 7th Biannual SGA Meeting, Athens, Greece, August 24-28, 2003.

Kouzmanov, K., Ivăşcanu, P., O'Connor, G., 2005. Porphyry Cu-Au and epithermal Au-Ag deposits in the southern Apuseni Mountains, Romania. South Apuseni Mountains district: Lat. 46 degrees 03'N, Long. 22 degrees 58'E. Ore Geology Reviews, 27, 46-47. DOI: 10.1016/j.oregeorev.2005.07.030

Loftus-Hills, G., Solomon, M., 1967. Cobalt, nickel and selenium in sulphides as indicators of ore genesis. Mineral Deposita, 2, 228-242.

Maydagan, L., Franchini, M., Lentz, D., Pons, J., McFarlane, C., 2013. Sulfide composition and isotopic signature of the Altar Cu-Au deposit, Argentina: constraints on the evolution of the porphyry-epithermal system. The Canadian Mineralogist, 51(6), 813-840. DOI: 10.3749/canmin.51.6.813

Milu, V., Leroy, J.L., Piantone, P., 2003. The Bolcana Cu–Au ore deposit (Metaliferi Mts., Romania) first data on the alteration and related mineralization: Comptes Rendus Geoscience, 335, 671-680. DOI: 10.1016/S1631-0713(03)00120-2

Milu, V., Milesi, J.-P., Leroy, J.L., 2004. Roşia Poieni copper deposit, Apuseni Mountains, Romania: advanced argillic overprint of a porphyry system. Mineralium Deposita, 39, 173-188. DOI: 10.1007/s00126-003-0390-z

Naglik, B., Tomasz, T., Dumańska-Słowik, M., Dimitrova, D., Derkowski, P., Zieliński, P., Habryn, R., Nadłonek, W., 2022. Multi-stage ore forming history of the Variscan porphyry Mo-Cu-W Myszkow deposit (Poland): Evidence from trace elements of pyrite. Ore Geology Reviews, 150, 105185. DOI: https://doi.org/10.1016/j.oregeorev.2022.10518

Neubauer, F., Lips, A., Kouzmanov, K., Lexa, J., Ivăşcanu, P., 2005. Subduction, slab detachment and mineralization: The Neogene in the Apuseni Mountains and Carpathians. Ore Geology Reviews, 27, 13-44. DOI: https://doi.org/10.1016/j.oregeorev.2005.07.002

Pačevski, A., Moritz, R., Kouzmanov, K., Marquard, K., Živković, P., Cvetković, L., 2012. Texture and composition of Pb-bearing pyrite from the Čoka Marin polymetallic deposit, Serbia, controlled by nanoscale inclusions. Canadian Mineralogist, 50, 1-20.

Pettke, T., Werner, E.H., MacIntosh, I., Heinrich, C.A., 2001. The porphyry to epithermal link: preliminary fluid chemical results from Roşia Poieni, Romania, and Famatina, Argentina. Romanian Journal of Mineral Deposits, 79, 81-82.

Pintea, I., 2001. Melt and fluid inclusions study in the Neogene porphyry Cu-Au (Mo) from Metaliferi Mountains. Romanian Journal of Mineral Deposits, Field Guidebook, 79(2), 28-29.

Raymond, O.L., 1996. Pyrite composition and ore genesis in the Prince Lyell copper deposit, Mt. Lyell mineral field, western Tasmania, Australia. Ore Geology Reviews, 10, 231-250.

Reich, M., Kesler, S.E., Utsunomiya, S., Palenik, C.S., Chryssoulis, S.L., Ewing, R.C., 2005. Solubility of gold in arsenian pyrite. Geochimica et Cosmochimica Acta, 69, 2781-2796. DOI: 10.1016/j.gca.2005.01.011

Reich, M., Deditius, A., Chryssoulis, S., Li, J.-W., Ma, C.-Q., Parada, M.A., Barra, F., Mittermayr, F., 2013. Pyrite as a record of hydrothermal fluid evolution in porphyry copper system: a SIMS/EMPA trace element study. Geochimica et Cosmochimica Acta, 104, 42-62. DOI: https://doi.org/10.1016/j.gca.2012.11.006

Reich, M., Large, R., Deditius, A., 2017. New advances in trace element geochemistry of ore minerals and accessory phases. Ore Geology Reviews, 87, 1215-1217. DOI: 10.1016/j.oregeorev.2016.10.020

Reich, M., Román, N., Barra, F., Morata, D., 2020. Silver-Rich Chalcopyrite from the Active Cerro Pabellón Geothermal System, Northern Chile. Minerals, 10, 113. DOI: https://doi.org/10.3390/min10020113

Rivas-Romero, C., Reich, M., Barra, F., Gregory, D., Pichott, S., 2021. The Relation between trace element composition of Cu-(Fe) sulfides and hydrothermal alteration in a porphyry copper deposit: Insights from the Chuquicamata underground mine, Chile. Minerals, 11, 671. DOI: https://doi.org/10.3390/min11070671

Roşu, E., Szakacs, A., Downes, H., Seghedi, I., Peckskay, Z., 2004. Timing of Miocene- Quaternary magmatism and metallogeny in the South Apuseni Mountains, Romania. Romanian Journal of Mineral Deposits, 8, 33-38.

Săndulescu, M., Kräutner, H., Borcoş, M., Năstăseanu, S., Patrulius, D., Ştefănescu, M., Ghenea, C., Lupu, M., Savu, H., Bercia, I., Marinescu, F., 1978. Geological map of Romania 1:1.000.000 in Geological Atlas, sheet no.1, published by Geological Institute of Romania.

Seghedi, I., Ntaflos, T., Pécskay, Z., Cristian Panaiotu, C., Mirea, V., Downes, H., 2022. Miocene extension and magma generation in the Apuseni Mts. (western Romania): a review. International Geology Review, 64(13), 1885-1911, DOI: 10.1080/00206814.2021.1962416

Sillitoe, R.H., 2010. Porphyry copper systems. Economic Geology, 105, 3-41. DOI: https://doi.org/10.2113/gsecongeo.105.1.3

Simon, G., Kesler, S., Essene, J.E., Chryssoulis, L.S., 2000. Gold in Porphyry Copper Deposits: Experimental Determination of the Distribution of Gold in the Cu-Fe-S System at 400° to 700°C. Economic Geology, 95, 259-270.

Sinclair, W.D., 2007. Porphyry deposits. in Geological Association of Canada, Mineral Deposits Division Mineral Deposits of Canada, Special Publication 5, A Synthesis of Major Deposit Types, District Metallogeny, the Evolution of Geological Provinces and Exploration Methods, 223-243.

Sykora, S., Cooke, D., Meffre, S., Stephanov, A.S., Gardner, K., Scott, R., Selley, D., Harris, A., 2018. Evolution of Pyrite Trace Element Compositions from Porphyry-Style and Epithermal Conditions at the Lihir Gold Deposit: Implications for Ore Genesis and Mineral Processing. Economic Geology, 113, 193-208. DOI: 10.382/econgeo.2018.45480361-0128/18/193-16

Tang, Y., Sun D., Gou, J., Ni, X., Zeng, X., Zhang, X., Liu, W., Liang, S., Deng, C., 2025, Chalcopyrite geochemistry: Advancements and implications in ore deposit research. Ore Geology Reviews, 179, 106528. DOI: ttps://doi.org/10.1016/j.oregeorev.2025.106528

Warr, LN., 2021. IMA–CNMNC approved mineral symbols. Mineralogical Magazine, 85(3), 291-320. DOI: 10.1180/mgm.2021.43

Winderbaum, L., Ciobanu, C.L., Cook, N.J.et al., 2012. Multivariate Analysis of an LA-ICP-MS Trace Element Dataset for Pyrite. Math. Geosci. 44, 823-842. DOI: https://doi.org/10.1007/s11004-012-9418-1

Manuscript received November 2024;
revision accepted September 2025;
published Online December 2025.